Journal of Nuclear Materials 389 (2009) 297–302

Contents lists available at ScienceDirect

Journal of Nuclear Materials

journal homepage: www.elsevier.com/locate/jnucmat

Radiation effects in cubic zirconia: A model system for ceramic oxides

L. Thomé [a,*], S. Moll [a], G. Sattonnay [b], L. Vincent [a], F. Garrido [a], J. Jagielski [c]

[a] Centre de Spectrométrie Nucléaire et de Spectrométrie de Masse, CNRS/IN2P3, Université Paris-Sud, Bât. 108, 91405 Orsay, France
[b] LEMHE/ICMMO, UMR 8182, Bât. 410, Université Paris-Sud, 91405 Orsay, France
[c] Institute for Electronic Materials Technology, Wolczynska 133, 01-919 Warsaw, Poland, and the Andrzej Soltan Institute for Nuclear Studies, 05-400 Swierk/Otwock, Poland

ARTICLE INFO

PACS:
61.80.–x
61.80.Jh
61.82.Ms
61.43.–j
61.85.+p
68.37.Lp

ABSTRACT

Ceramics are key engineering materials for electronic, space and nuclear industry. Some of them are promising matrices for the immobilization and/or transmutation of radioactive waste. Cubic zirconia is a model system for the study of radiation effects in ceramic oxides. Ion beams are very efficient tools for the simulation of the radiations produced in nuclear reactors or in storage form. In this article, we summarize the work made by combining advanced techniques (RBS/C, XRD, TEM, AFM) to study the structural modifications produced in ion-irradiated cubic zirconia single crystals. Ions with energies in the MeV–GeV range allow exploring the nuclear collision and electronic excitation regimes. At low energy, where ballistic effects dominate, the damage exhibits a peak around the ion projected range; it accumulates with a double-step process by the formation of a dislocation network. At high energy, where electronic excitations are favored, the damage profiles are rather flat up to several micrometers; the damage accumulation is monotonous (one step) and occurs through the creation and overlap of ion tracks. These results may be generalized to many nuclear ceramics.

1. Context of the study

The management of radioactive waste produced in nuclear power plants is a crucial problem facing developed countries. The long history of research on this topic has shown that crystalline ceramics are among the most promising materials for use as matrices for the immobilization and/or transmutation of nuclear waste. A primordial and challenging issue for the qualification of nuclear matrices is the study of their stability in a radiative environment. Radiation produced in nuclear reactors or in storage forms may be simulated by external irradiations with various types of ions in a broad energy range. Actually low energy heavy ions account for the recoil nuclei arising from the α-decay of actinides, and swift ions aim to reproduce the impact of fission fragments. Moreover, besides an obvious societal interest, ion irradiation of ceramics may advance the understanding of the fundamental mechanisms of damage production by either nuclear collisions at low energy or electronic excitations at high energy.

The topic concerning the effects of radiation in nuclear ceramics is so broad that it requires a whole book to do it justice. The state of knowledge was regularly upgraded in thorough reviews [1–8]. To deal with this issue in a short article, we will focus the demonstration on the test case of cubic zirconia (CZ) which is a model system for ceramic oxides [9–16]. The results reported here constitute a small part of a broader work which is devoted to the comparison of the damage induced in CZ single crystals irradiated with heavy ions in a wide energy range (from a few MeV to a few GeV) in order to explore nuclear collision (Section 2) and electronic excitation (Section 3) regimes. The depth distribution, the degree and the nature of the damage induced by ion irradiation were measured as a function of the ion fluence by combining Rutherford backscattering and channeling spectrometry (RBS/C), X-ray diffraction (XRD), transmission electron microscopy (TEM) and atomic force microscopy (AFM).

2. Effects of elastic collisions

The basic process of nuclear energy loss (S_n) in solids, which is dominant at low ion energy (i.e. below ~10 keV/u), is the creation of collision cascades by primary knock-on atoms. Cascades are responsible for a large variety of structural modifications (topological or chemical disorder, swelling, phase transformations, amorphization, etc.) which depend on several key parameters, such as the target material, the irradiation temperature, and the fluence flux, and energy of the ions. The examples provided in this section deal with irradiation of CZ at room temperature using 4 MeV Au ions provided by the JANNUS facility in Orsay.

Basically the damage depth distribution in ion-irradiated single crystals can be determined from the analysis of the damage-induced dechanneling exhibited in RBS spectra recorded along a major axis direction (see an example in Fig. 1(a)). Among the methods

* Corresponding author.
E-mail address: thome@csnsm.in2p3.fr (L. Thomé).

0022-3115/$ - see front matter © 2009 Elsevier B.V. All rights reserved.
doi:10.1016/j.jnucmat.2009.02.013

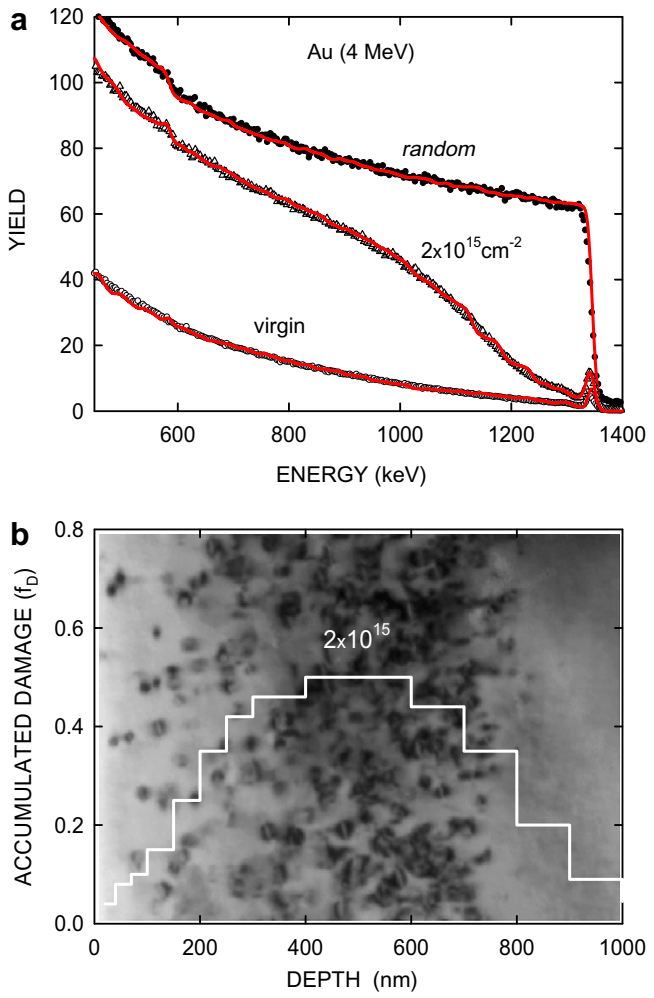

Fig. 1. (a) RBS spectra recorded in random (filled circles) and ⟨100⟩-axial (open symbols) directions on a CZ crystal irradiated with 4 MeV Au ions. Analyzing particles: 1.6 MeV ^{4}He ions. Solid lines are simulations of RBS/C data with the Monte-Carlo McChasy code [18]. (b) Comparison of the damage depth distributions determined by TEM (micrograph) and RBS/C (histogram) for a CZ crystal irradiated with 4 MeV Au ions at a fluence of 2×10^{15} cm^{-2}. The vertical scale refers to values of f_D obtained by Monte-Carlo simulations of RBS/C data.

which can be used for this analysis, Monte-Carlo simulations of aligned RBS spectra offer the best accuracy [17]. An illustration of the use of a Monte-Carlo code (McChasy [18]) is provided in Fig. 1. Fig. 1(a) shows fits to RBS/C spectra (solid lines), and Fig. 1(b) compares the result obtained by this simulation (histogram) with a TEM micrograph recorded on a cross-sectional thin layer taken from the same sample. A very good agreement is observed between the two techniques. A reasonable agreement is also obtained with TRIM calculations [19] which predict that the damage due to ballistic collisions exhibit gaussian-like shapes with a maximum not far from that observed experimentally.

A typical variation of the accumulated damage (f_D) with the ion fluence is represented in Fig. 2. Two steps are clearly exhibited: (1) the creation of a low amount of damage ($f_D < 0.10$) at small ion fluences (below $\sim 10^{15}$ cm^{-2}); (2) a sharp rise of the damage level over a short fluence range (from $\sim 10^{15}$ till 2–3 $\times$ 10^{15} cm^{-2}) followed by saturation at higher fluences. The insets of Fig. 2 show TEM micrographs performed on samples irradiated at fluences characteristic of the two damage steps. Individual dislocation loops are clearly formed during step 1, whereas a network of tangle dislocations appears during step 2.

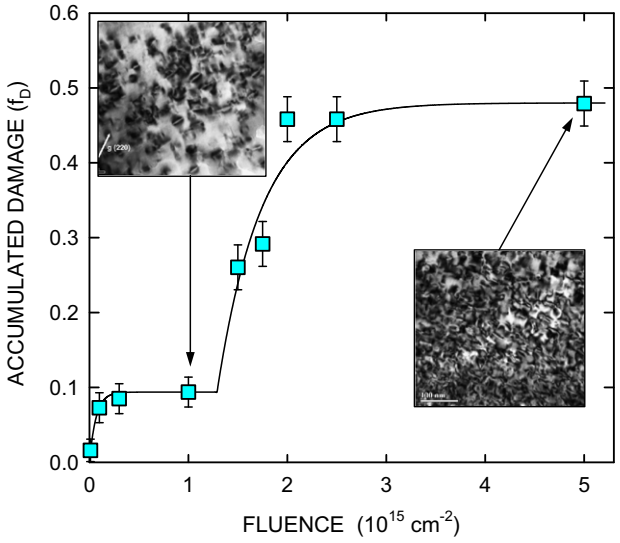

Fig. 2. Accumulated damage (f_D) vs ion fluence in CZ crystals irradiated with 4 MeV Au ions. The solid line is a fit to RBS/C data using the MSDA model [20] with $n = 2$. Insets show TEM micrographs on CZ crystals irradiated at fluences indicated by the arrows.

The damage build-up in ion-irradiated solids may be reproduced in the framework of a model (referred to as MSDA [20]) based on the assumptions that: (i) the damage accumulation process occurs in several steps, (ii) each step is triggered by the destabilization of the current structure of the material, (iii) the structural transformations are described by a direct impact mechanism. According to the MSDA model the variation of f_D with the ion fluence Φ is represented by the equation [20]:

$$f_D = \sum_{i=1}^{n} \left(f_{D,i}^{\mathrm{sat}} - f_{D,i-1}^{\mathrm{sat}} \right) G[1 - \exp(-\sigma_i(\Phi - \Phi_{i-1}))], \qquad (1)$$

where n is the number of steps required to describe the disordering process, $f_{D,i}^{\mathrm{sat}}$ is the level of damage at saturation in the ith step; σ_i is the cross-section for damage formation in the ith step, G is a *ad-hoc* function which transforms negative values into 0 and leaves positive values unchanged. The accumulated damage obtained from RBS/C data in the case of CZ irradiated with 4 MeV Au ions is nicely reproduced (solid line in Fig. 2) using Eq. (1) with $n = 2$ (two-step process). It is worth noting that the MSDA model may account for most of the damage kinetics reported in the literature for ion-irradiated materials [20].The evolution of the microstructure of irradiated crystals may also be determined by XRD experiments. Fig. 3 presents a remarkable example of the correlation which may be obtained between RBS/C and XRD results. It shows the variation with the ion fluence (and also with the number of dpa produced by elastic collisions) of the accumulated damage f_D (Fig. 3(a)-RBS/C), of the lattice parameter a (Fig. 3(b)-XRD), and of the generated stress s (Fig. 3(c)-XRD) in a CZ crystal irradiated with 4 MeV Au ions. A small regular increase of f_D, a and s is observed in step 1 (i.e. up to $\sim$5 dpa), whereas a sharp drop of a and s, correlated with the sharp increase of f_D, is observed in step 2 (above $\sim$5 dpa). Thus, it can be concluded from the comparison of RBS/C, XRD and TEM data that the formation of dislocation loops during step 1 induces an increase of the lattice parameter and of the stress, while the formation of a network of tangle dislocations during step 2 leads to a decrease of the lattice parameter and to a relaxation of the stress. The same behavior is observed in CZ irradiated with a large variety of low energy ions [13], leading to the conclusion that the number of dpa is the key parameter for the evolution of the damage build-up in the nuclear collision regime. Similar results are also obtained

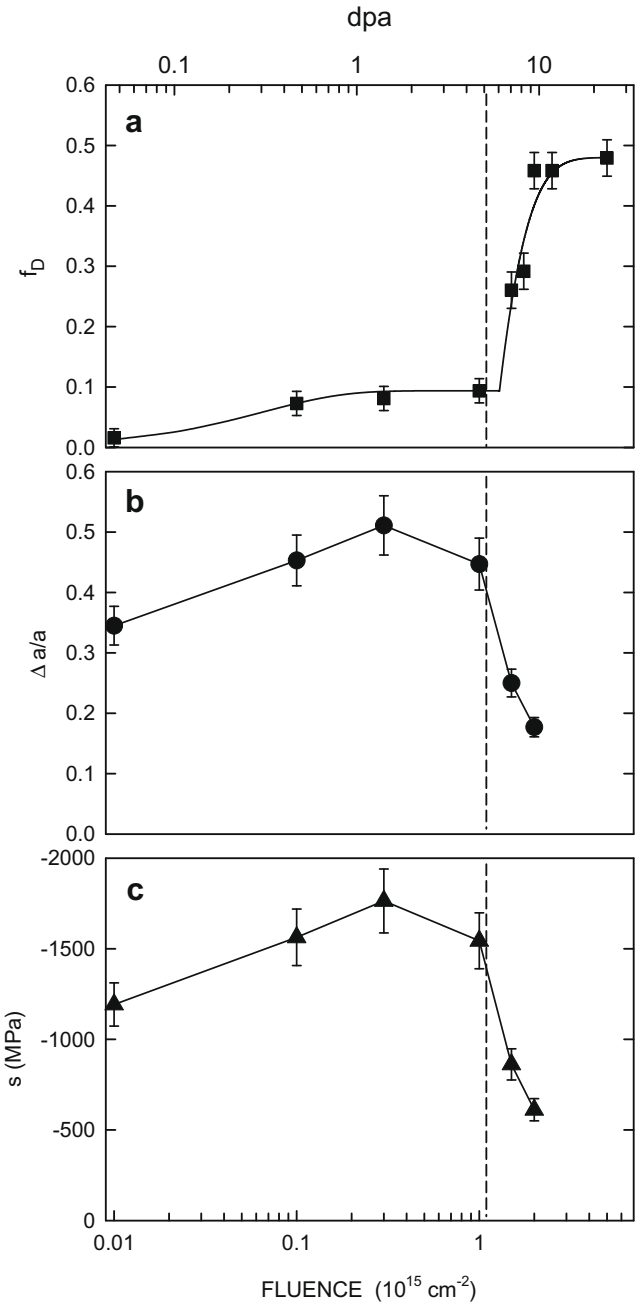

Fig. 3. Accumulated damage (f_D) measured by RBS/C (a) and lattice parameter ($\Delta a/a$) and stress (s) measured by XRD (b) and (c) vs the ion fluence and the number of dpa for CZ crystals irradiated with 4 MeV Au ions.

in other non-amorphizable ceramics (for instance spinel and uranium dioxide) irradiated at low energy [21–28].

3. Effects of electronic excitation

The high electronic energy deposition (S_e) due to the passage of a swift ion (i.e. above ~1 MeV/u) induces the formation of an electrostatically unstable cylinder of ionized atoms (track) and the emission of electrons. Different models were developed to account for the resulting atomic rearrangements, depending on whether the attention is focused on the process by which the energy of electrons is dissipated in the lattice (thermal spike) [29–31] or on the response of the ionized atoms (Coulomb-explosion) [32–34]. The morphology of ion tracks depends on the value of S_e [35]: spherical defects appear at low S_e, whereas discontinuous or continuous cylinders are formed at high S_e. It was also generally shown that the track radius increases with increasing S_e. The structure of the material inside each individual track is dependent on both the irradiating ion (through the deposited energy density) and the investigated material. There have been only limited studies on the evolution of the microstructure of nuclear ceramics submitted to swift ion irradiation and additional data are still needed for a complete understanding of the basic phenomena. The examples provided in this section deal with irradiations of CZ at room temperature using 940 MeV Pb ions provided by the GANIL accelerator in Caen.

The depth distribution of the damage induced by swift ion irradiation can be determined from RBS/C spectra (Fig. 4), provided that computer codes are used to fit the data [17]. Fig. 4(a) shows fits to RBS/C spectra (solid lines) with the McChasy code [18], and Fig. 4(b) compares a typical damage profile obtained by RBS/C (histogram) with a TEM micrograph recorded on a cross-sectional thin layer taken from the same sample. Here again a good agreement is obtained between the two techniques. The damage depth distribution exhibits three main regions: (i) a huge disorder at low depth (up to 60–70 nm); (ii) a decrease of the amount of defects in a small depth interval around 100 nm; (iii) a rather constant damage yield beyond 200 nm which extends up to the

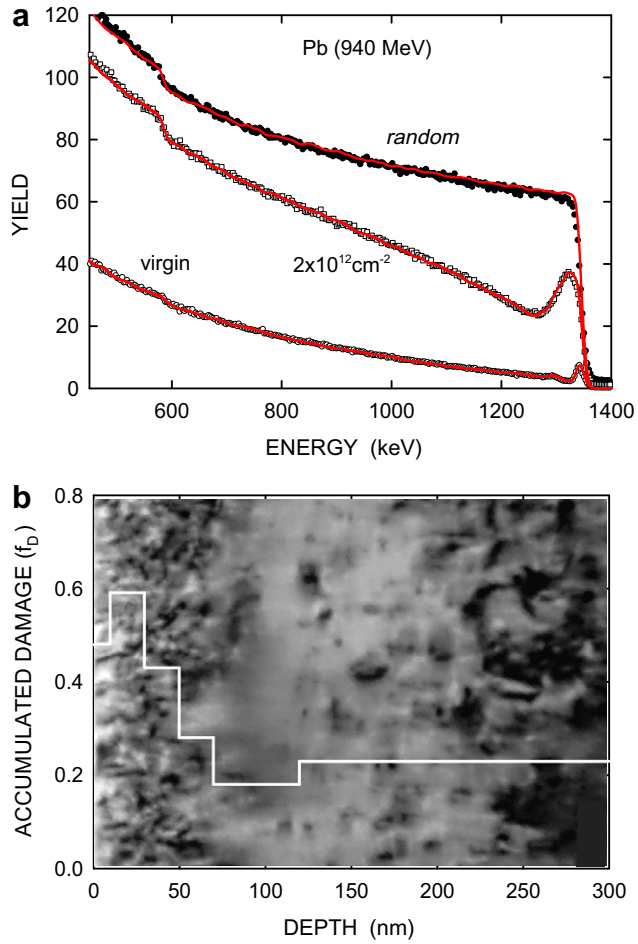

Fig. 4. (a) RBS spectra recorded in random (filled circles) and ⟨100⟩-axial (open symbols) directions on a CZ crystal irradiated with 940 MeV Pb ions. Analyzing particles: 1.6 MeV ^{4}He ions. Solid lines are simulations of RBS/C data with the Monte-Carlo McChasy code [18]. (b) Comparison of the damage depth distributions determined by TEM (micrograph) and RBS/C (histogram) for a CZ crystal irradiated with 940 MeV Pb ions at a fluence of 2×10^{12} cm^{-2}. The vertical scale refers to values of f_D obtained by Monte-Carlo simulations of RBS/C data.

maximum analyzed depth (~2 μm) in RBS/C (not seen on the figure). Thus, the damage profiles measured on crystals irradiated at high energy are very different from those measured on crystals irradiated at low energy (Fig. 1(b)), and they also differ from the electronic energy deposition calculated with the TRIM code [19] which is almost flat from the sample surface up to a depth of a few micrometers.

The variation of the steady value (i.e. at a depth higher than 200 nm) of the accumulated damage (f_D) with the ion fluence is represented in Fig. 5 for the same irradiation conditions. The damage build-up may be reproduced in the framework of the MSDA model with $n = 1$ (single-step process). This result can be accounted for by considering that the melting of highly-ionized matter in cylindrical ion tracks induced by electronic excitation leads to a direct transformation of the melt volume into a new structure. The diameter of ion tracks, d_{RBS}, may be deduced from the value of σ in Eq. (1): $d_{RBS} = 5.8 \pm 1.0$ nm for 940 MeV Pb ions in CZ. A direct visualization of ion tracks is possible by using TEM and AFM (see insets in Fig. 5) on samples irradiated at low fluences (below 10^{12} cm^{-2}). From the TEM micrograph the value of the inner track diameter is $d_{TEM} = 4$ nm, i.e. in reasonable agreement with d_{RBS}. The AFM micrograph shows that irradiation has led to the formation of hillocks which are randomly distributed over the whole sample surface. The mean height of hillocks is ~2 nm and their mean diameter $d_{AFM} = 30$ nm (with a tip width of ~10 nm). The discrepancy between the diameter of the hillocks observed by AFM probing the sample surface and the diameter of the tracks obtained by methods which probe the sample bulk (TEM and RBS/C) may be understood in the framework of the thermal spike model [29–31]. The inner ion track (observed by TEM) is due to the melting of the material in the wake of an incident ion. The molten matter is thus ejected towards the crystal surface and form the cones observed by AFM.

When the ion fluence is increased above 10^{12} cm^{-2}, individual tracks overlap and a specific microstructure is formed in the material. The surface of the sample is strongly damaged (i.e. more than the bulk), due to the overlapping of hillocks shown in Fig. 5. This feature could be an explanation for the huge disorder observed by RBS/C in the region close to the sample surface (Fig. 4). XRD was used to elicit the micro-structural modifications and/or the phase transformations induced at high fluences. The analysis of the broadening upon irradiation of standard (θ–2θ) scans and of rocking curves (ω-scans) indicates that: (i) irradiation has led to a swelling (increase of the lattice parameter) which increases almost linearly with increasing ion fluence; (ii) coherent diffraction domains with a size D and an out-of-plane disorientation angle α are formed upon irradiation. Fig. 6(a) and (b) show that the value of D decreases, whereas the value of α increases with increasing ion fluence. Above 10^{13} cm^{-2} a clear effect of saturation is observed for the parameters extracted from the analysis of both RBS/C and XRD data. This saturation is an indication that the material has reached an equilibrium state and that further irradiation will not modify substantially the structure of the crystals (no amorphization).

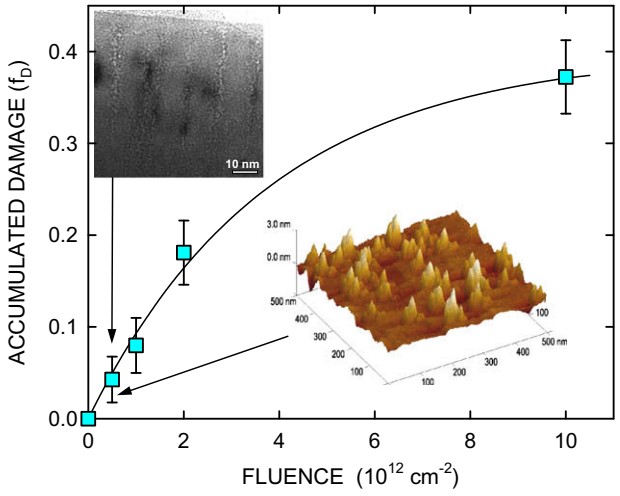

Fig. 5. Accumulated damage (f_D) *vs* the ion fluence in CZ crystals irradiated with 940 MeV Pb ions. The solid line is a fit to RBS/C data using the MSDA model [20] with $n = 1$. Insets show TEM (upper-left corner) and AFM (lower-right corner) micrographs on a CZ crystal irradiated at a fluence of 10^{10} cm^{-2}.

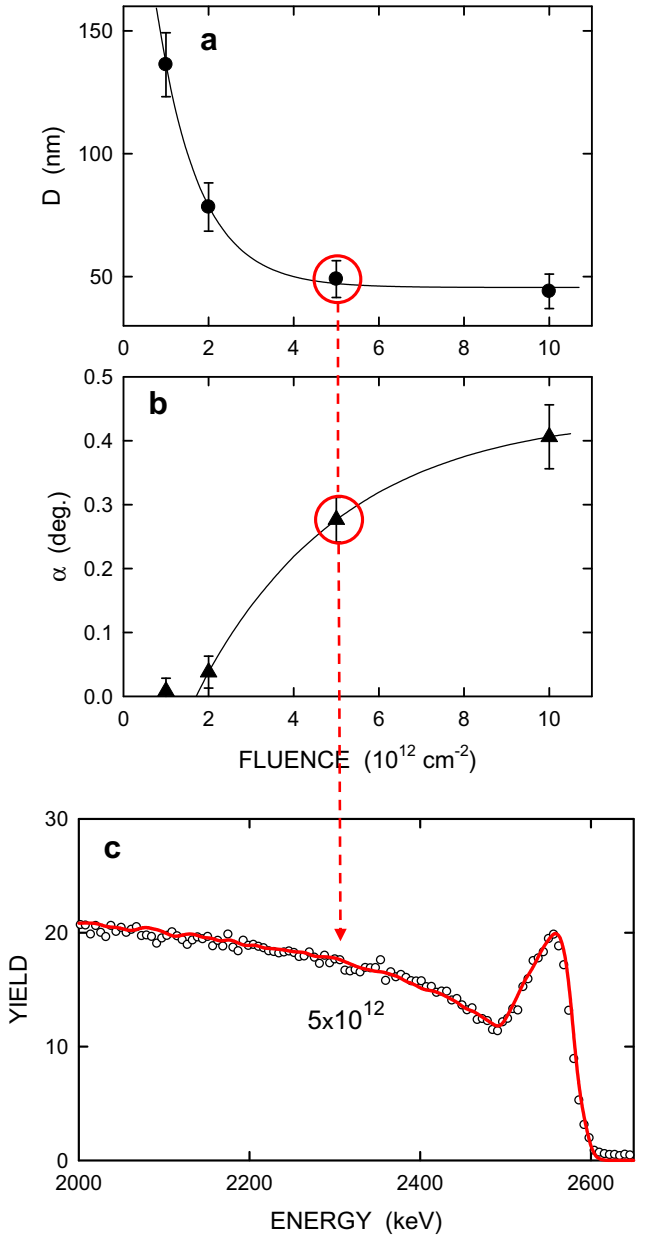

Fig. 6. (a) and (b) Size of micro-domains (D) and disorientation angle (α) measured by XRD *vs* ion fluence for CZ crystals irradiated with 940 MeV Pb ions. (c) RBS/C spectrum recorded in the ⟨100⟩-axial direction (open circles) on a CZ crystal irradiated with 940 MeV Pb ions at a fluence of 5×10^{12} cm^{-2}, and fit to this spectrum (solid line) with the Monte-Carlo McChasy code [18] assuming the creation of micro-domains with a size and a disorientation angle taken from (a) and (b) (circled values).

XRD results may be cross-checked by analyzing RBS/C data with the McChasy code with the assumption that single crystals are subdivided upon irradiation into small grains (size D) disoriented (by an angle α) with respect to the main crystallographic direction. Additional disorder is introduced in the sub-surface layer to account for the huge damage peak exhibited in this region on aligned RBS spectra. Fig. 6(c) shows the best fit to data obtained on the sample irradiated with 940 MeV Pb ions at a fluence of 5×10^{12} cm^{-2}, which provides values of the grain size $D = 60$ nm and of the disorientation angle $\alpha = 0.26$, i.e. in good agreement with XRD results (Fig. 6(a) and (b)).

4. Concluding remarks

Cubic zirconia is a model system for the study of radiation effects in ceramic oxides. Experimentally, ions with energies in the MeV–GeV range may be used to simulate the radiations produced in nuclear reactors or in storage forms. From a fundamental point of view they allow exploring separately the nuclear collision and electronic excitation regimes. The depth distribution, the degree and the nature of the damage, as well as the microstructure modifications produced in ion-irradiated cubic zirconia single crystals, were measured as a function of the ion fluence by combining advanced techniques which probe the sample at various spatial scales (RBS/C, XRD, TEM, AFM).

At low energy (4 MeV Au ions) the damage distributions fit the nuclear energy deposition; a disorder peak is exhibited around the ion projected range (~500 nm). At high energy (940 MeV Pb ions) the damage distributions fit the electronic energy loss; the profile of defects is rather flat up to a depth of several micrometers (with an enhanced disorder in the near-surface region). The damage kinetics, summarized on Fig. 7 in both cases where S_n or S_e are dominant, were satisfactorily represented in the framework of a multi-step damage accumulation model (MSDA) previously developed to account for the damage production in irradiated solids. The shape of the build-up and the fluence range where the damage appears strongly depend on the ion slowing-down regime.

Tracks created by electronic excitation at high energy likely lead to a direct transformation of the melt volume into a new structure via a single-step process. The diameters of ion tracks indirectly determined from RBS/C data agree with those directly measured on TEM micrograph. Larger hillocks of matter ejected from the ion tracks are observed by AFM. The overlapping of tracks at high fluences leads to the fragmentation of the single crystal in slightly disoriented micro-crystallites. In the case of heavy ion irradiation (Pb) a saturation of the damage is observed above 10^{13} cm^{-2}. TEM and RBS/C data have also evidenced the existence of a S_e threshold for track formation at 10–20 keV/nm.

The damage cascades created by nuclear collisions at low energy lead to several steps of disorder accumulation due to the formation and relaxation of radiation-induced stresses. A sharp increase of the damage is exhibited in the second step, due to the formation of a network of tangled dislocations revealed by TEM. This second step occurs when a radiation dose of a few dpa is achieved independently of the irradiating ion, corresponding to a fluence by several orders of magnitude higher (~10^{15} cm^{-2}) than that required to obtain the same amount of disorder at high energy (1013 cm^{-2}). A saturation of the damage is also observed around 10^{16} cm^{-2} for heavy ion irradiation (Au).

Finally, two remarkable features may be noticed: (i) the various irradiations never lead to the creation of a total disorder (such as amorphization) at the highest fluences used in the experiments; (ii) the damage behavior of cubic zirconia is very similar to that of several counterparts (for instance spinel and uranium dioxide). The former point shows that oxide ceramics with the fluorite-type structure are materials very resistant against ion irradiation, and are in that sense adequate materials for immobilization or transmutation matrices. Future prospects in this research field could be the investigation of the synergy between radiation effects induced by low and high energy ions. Such a daunting challenge will be reachable by the development of dedicated new facilities able to deliver several ion beams in a common irradiation chamber, such as the JANNUS platform under construction in the Orsay–Saclay area [36].

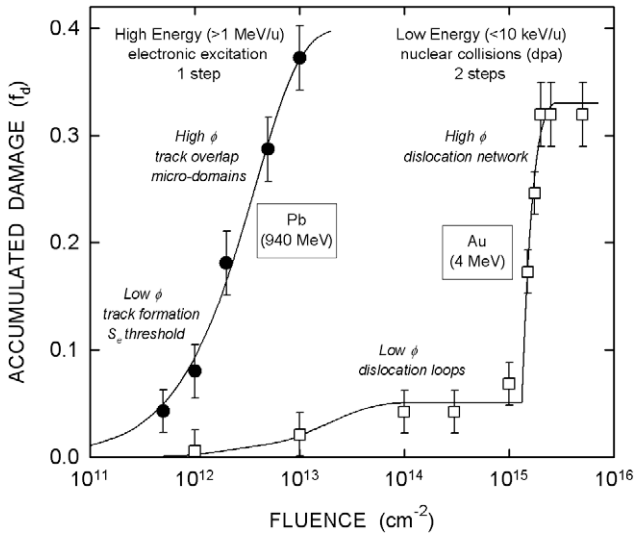

Fig. 7. Comparison of the damage build-up obtained for CZ crystals irradiated with 4 MeV Au (squares) and 940 MeV Pb (circles) ions. Lines are fits to data using the MSDA model [20].

Acknowledgments

We like to thank the JANNUS-Orsay staff for assistance during low-energy irradiations and RBS/C experiments, and the GANIL-Caen staff for assistance during high-energy irradiations. This work was partially financed by the GNRs NOMADE and MATINEX. The experimental program benefited from grants provided by the French–Polish cooperation program n°01-104.

References

[1] Hj. Matzke, Radiat. Eff. 64 (1982) 3.
[2] L.W. Hobbs, F.W. Clinard Jr., S.J. Zinkle, R.C. Ewing, J. Nucl. Mater. 216 (1994) 291.
[3] R.C. Ewing, W.J. Weber, F.W. Clinard Jr., Prog. Nucl. Energy 29 (1995) 63.
[4] S.J. Zinkle, C. Kinoshita, J. Nucl. Mater. 251 (1997) 200.
[5] C.J. Mc Hargue, Mater. Sci. Eng. A 253 (1998) 94.
[6] W.J. Weber, R.C. Ewing, C.R.A. Catlow, T. Diaz de la Rubia, L.W. Hobbs, C. Kinoshita, Hj. Matzke, A.T. Motta, M. Nastasi, E.K.H. Salje, E.R. Vance, S.J. Zinkle, J. Mater. Res. 13 (1998) 1434.
[7] W.L. Gong, W. Lutze, R.C. Ewing, J. Nucl. Mater. 277 (2000) 239.
[8] R.C. Ewing, W.J. Weber, J. Lian, J. Appl. Phys. 95 (2004) 5949.
[9] N. Yu, K.E. Sickafus, P. Kodali, M. Nastasi, J. Nucl. Mater. 244 (1997) 1434.
[10] C. Degueldre, J.M. Paratte, Nucl. Technol. 123 (1998) 21.
[11] K.E. Sickafus, Hj. Matzke, Th. Hartmann, K. Yasuda, J.A. Valdez, P. Chodak III, M. Nastasi, R.A. Verall, J. Nucl. Mater. 274 (1999) 66.
[12] L.M. Wang, S.X. Wang, R.C. Ewing, Phil. Mag. Lett. 80 (2000) 341.
[13] L. Thomé, J. Fradin, J. Jagielski, A. Gentils, S.E. Enescu, F. Garrido, Eur. Phys. J. Appl. Phys. 24 (2003) 37.
[14] G. Sattonnay, L. Thomé, J. Nucl. Mater. 348 (2006) 223.
[15] J.M. Costantini, C. Trautmann, L. Thomé, J. Jagielski, F. Beuneu, J. Appl. Phys. 101 (2007) 073501.
[16] S. Zhu, S.X. Wang, L.M. Wang, R.C. Ewing, X.T. Zu, Appl. Phys. Lett. 90 (2007) 171915.
[17] L. Thomé, J. Jagielski, L. Nowicki, A. Turos, A. Gentils, F. Garrido, Vacuum 78 (2005) 401.
[18] L. Nowicki, Ph.D. Thesis, The Andrzej Soltan Institute for Nuclear Studies, Warsaw, 1997.

[19] J.F. Ziegler, J.P. Biersack, U. Littmark, in: J.F. Ziegler (Ed.), The Stopping and Range of Ions in Solids, vol. 1, Springer, Berlin, 1985.
[20] J. Jagielski, L. Thomé, Vacuum 81 (2007) 1352.
[21] S.E. Enescu, L. Thomé, A. Gentils, T. Thomé, J. Mater. Res. 19 (2004) 3463.
[22] A. Gentils, S.E. Enescu, L. Thomé, H. Khodja, G. Blaise, T. Thomé, J. Appl. Phys. 97 (2005) 113509.
[23] F. Garrido, C. Choffel, J.C. Dran, L. Thomé, L. Nowicki, A. Turos, Nucl. Instrum. and Meth. B 127&128 (1997) 634.
[24] F. Garrido, L. Vincent, G. Sattonnay, L. Nowicki, L. Thomé, Nucl. Instrum. and Meth. 266 (2008) 2842.
[25] N. Bordes, K.E. Sickafus, E.A. Cooper, R.C. Ewing, J. Nucl. Mater. 225 (1995) 318.
[26] N. Bordes, L.M. Wang, R.C. Ewing, K.E. Sickafus, J. Mater. Res. 10 (1995) 981.
[27] L.M. Wang, W.L. Gong, S.X. Wang, R.C. Ewing, J. Am. Ceram. Soc. 82 (1999) 3321.
[28] L.M. Wang, S. Zhu, S.X. Wang, R.C. Ewing, N. Boucharat, A. Fernandez, Hj. Matzke, Prog. Nucl. Energy 38 (2001) 295.
[29] M. Toulemonde, C. Dufour, E. Paumier, Phys. Rev. B 46 (1992) 14362.
[30] G. Szenes, Phys. Rev. B 51 (1995) 8026.
[31] H. Trinkaus, A.I. Ryazanov, Phys. Rev. Lett. 74 (1995) 5072.
[32] R.L. Fleischer, P.B. Price, R.M. Walker, J. Appl. Phys. 36 (1965) 3645.
[33] L.E. Seiberling, J.E. Griffith, T.A. Tombrello, Radiat. Eff. 52 (1980) 201.
[34] D. Lesuer, A. Dunlop, Radiat. Eff. Def. Solids 126 (1993) 105.
[35] M. Toulemonde, Nucl. Instrum. and Met. B 156 (1999) 1.
[36] Y. Serruys, M.O. Ruault, P. Trocellier, S. Henry, O. Kaitasov, P. Trouslard, Nucl. Instrum. and Meth. B 240 (2005) 124.